IEEE Photonics Journal
An IEEE Photonics Society Publication

Open Access

Silicon Graphene Reconfigurable CROWS and SCISSORS

Volume 7, Number 2, April 2015

J. Capmany, Fellow, IEEE
D. Domenech
P. Muñoz

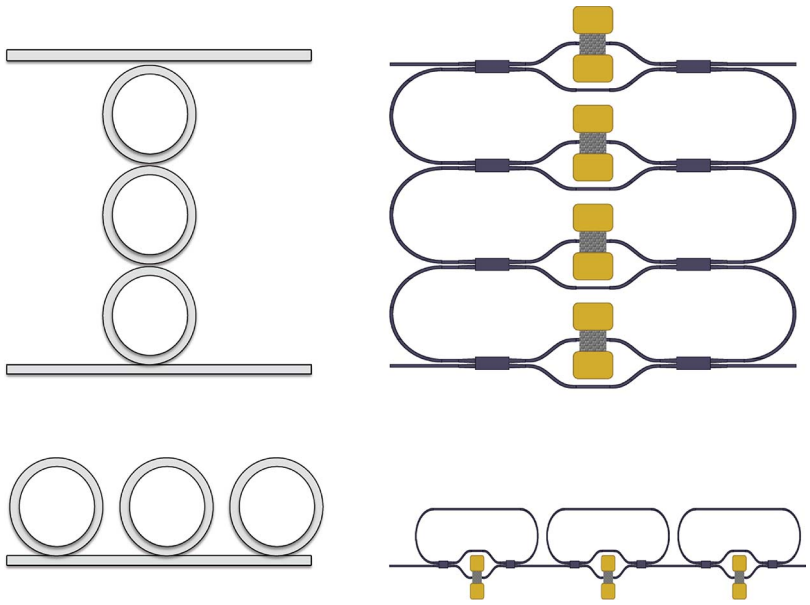

DOI: 10.1109/JPHOT.2015.2407314
1943-0655 © 2015 IEEE

Silicon Graphene Reconfigurable CROWS and SCISSORS

J. Capmany,[1] *Fellow, IEEE*, D. Domenech,[2] and P. Muñoz[1]

[1]ITEAM Research Institute, Universidad Politecnica de Valencia, 46022 Valencia, Spain
[2]VLC Photonics S.L., 46022 Valencia, Spain

DOI: 10.1109/JPHOT.2015.2407314
1943-0655 © 2015 IEEE. Translations and content mining are permitted for academic research only. Personal use is also permitted, but republication/redistribution requires IEEE permission. See http://www.ieee.org/publications_standards/publications/rights/index.html for more information.

Manuscript received January 27, 2015; revised February 19, 2015; accepted February 20, 2015. Date of publication February 26, 2015; date of current version March 11, 2015. Corresponding author: J. Capmany (e-mail: jcapmany@iteam.upv.es).

Abstract: We propose the incorporation of graphene to integrated coupled resonator waveguides and side-coupled integrated spaced sequence of resonator devices to enable reconfigurable operation. The key element to achieve this is a tunable silicon graphene Mach–Zehnder interferometer (MZI) that acts as an equivalent variable 2×2 coupler, where the value of its coupling constant is changed by varying the chemical potential of a graphene section placed on top of one of its arms.

Index Terms: Microwave photonics, microwave photonic filtering, integrated optics, graphene.

1. Introduction

Graphene is a 2-D single layer of carbon atoms arranged in an hexagonal lattice that has raised considerable interest in recent years due to its remarkable optical and electronic properties [1]–[3]. In particular, it has a linear dispersion relationship in the so-called Dirac points where electrons behave as fermions with zero mass, propagating at a speed of around 10^6 ms^{-1} and featuring mobility values of up to 10^6 $cm^2V^{-1}s^{-1}$. Graphene also shows unusual optical properties [4]. For instance, due to its linear dispersion, it can absorb light over a broad frequency range enabling broadband applications. Another noteworthy property of this material is that the density of states of carriers near the Dirac point is low, and as a consequence, its Fermi energy can be tuned significantly with relatively low electrical energy (applied voltage) [1]–[4]. This Fermi level tuning changes, in turn, the refractive index of graphene, and thus, the combination of graphene with integrated dielectric waveguides opens unprecedented possibilities for the design of tunable components in optoelectronics [5], and several groups have recently reported devices with applications in the microwave, terahertz, and photonic regions of the electromagnetic spectrum [3]–[6]. A particularly active area of research aims at designing tunable integrated photonic components and different groups have reported both theoretical and experimental contributions addressing different functionalities that include electro-absorption modulation in straight waveguides [6]–[8], resonant modulators [9], channel switching [10], and electro-refractive modulation [11].

Although most of the former components can find application in digital communications, the use of graphene can also be exploited in microwave photonics (MWP) applications, as we have recently proposed for the implementation of phase shifters [12] and true time delay lines, [13].

While these devices are key in most MWP systems [14], [15], these systems also require the availability of reconfigurable complex integrated resonant filters [16], such as coupled resonator optical waveguides (CROWS) and side-coupled integrated spaced sequence of resonators (SCISSORS). In this paper, we propose the incorporation of graphene to integrated coupled resonator waveguides (CROWS) and SCISSOR devices to enable reconfigurable operation. The paper is structured as follows. In Section 2 we review some basic properties of graphene that are important in the design of tunable integrated photonic components, such as the dependence of its conductivity and dielectric constant on the chemical potential and applied voltage and we briefly describe the silicon photonics waveguide considered for the implementation of the reconfigurable resonant filters. Although graphene can be incorporated into other material platforms including InP [17] and Si_3N_4 [18] its integration in Silicon waveguides is so far better understood both theoretically and experimentally, and therefore, we consider this option in the paper, although the design procedure can be extended to both of them as well. Section 3 presents the layouts of the CROW and SCISSOR devices and elaborates on the designs of its key component, which is the tunable 2×2 coupler implemented by means of a graphene based Mach–Zehnder Interferometer (MZI). It also presents the results obtained for the design of uniform and apodized CROW and SCISSOR reconfigurable devices and also describes the synthesis procedure to implement maximally flat Butterworth filters. Section 4 discusses practical orders of magnitude related to power voltage operation ranges, power consumption and reconfiguration speed of these filters. Section 5 presents our conclusions.

2. Graphene Conductivity and Silicon Waveguide Design

Graphene has noteworthy optical properties due to its conical band structure that allow both intra-band and inter-band transitions [1]–[3]. Both types of transitions contribute to the material conductivity [18]

$$\sigma(\omega) = \sigma_{\text{intra}}(\omega) + \sigma_{\text{inter}}(\omega). \tag{1}$$

Intra-band transitions are the dominant source for the overall conductivity in the microwave and terahertz regions of the spectrum that can be expressed in terms of the Kubo's formula [18]:

$$\sigma_{\text{intra}}(\omega) = \frac{ie^2 k_B T}{\pi \hbar^2 (\omega + i2\Gamma)} \left[\frac{\mu_c}{k_B T} + 2\ln\left(e^{-(\mu_c/k_B T)} + 1\right) \right] \tag{2}$$

where e represents the charge of the electron, $\hbar$ the angular Planck constant, k_B the Boltzmann constant, T the temperature, μ_c is the Fermi level or chemical potential

$$\Gamma = \frac{e\mathbf{v_F^2}}{\mu\mu_c} \tag{3}$$

is the electron collision rate which is a function of the electron mobility μ, and the Fermi velocity in graphene $\mathbf{v_F} \approx 10^6$ ms^{-1}. In the visible optical region of the spectrum, however, inter-band transitions dominate the conductivity that is given by [3]

$$\sigma_{\text{inter}}(\omega) = \frac{ie^2\omega}{\pi} \int_0^\infty \frac{f(x-\mu_c) - f(-x-\mu_c)}{4x^2 - (\hbar\omega + i\Gamma)^2} dx \tag{4}$$

where $f(x)$ is the Fermi-Dirac distribution. From (1)–(4), one can get the dielectric constant of a layer of graphene:

$$\varepsilon_g(\omega) = 1 + \frac{i\sigma(\omega)}{\omega\varepsilon_o\Delta} \tag{5}$$

where $\Delta = 0.34$ nm is the thickness of the layer. The upper left part of Fig. 1 represents, as an example, the real and imaginary parts of both the intra and inter-band conductivities for $\lambda = 1550$ nm,

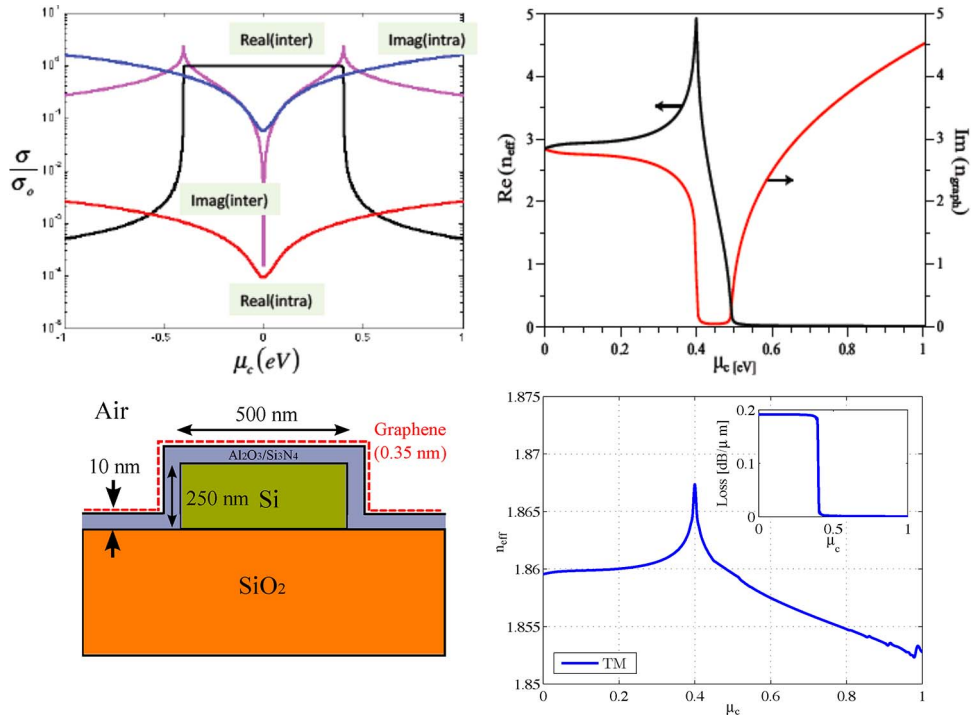

Fig. 1. Upper left: Real and imaginary parts of the intra- and inter-band conductivities of graphene for $\lambda = 1550$ nm, $T = 300\ ^\circ K$, and $1/2\Gamma = 5.10^{-13}$ sec. Upper right: Overall complex refractive index. Lower left: Deep silicon waveguide with a layer of graphene placed on top of it. Lower right: Effective index and losses for the TM mode of a deep graphene silicon waveguide.

$T = 300\ ^\circ$K, and $1/2\Gamma = 5.10^{-13}$ sec as a function of the chemical potential, while the lower part represents the dielectric constant. In this particular example, a transition can be observed at $|\mu_c| = 0.4$ eV, where the dielectric constant changes from purely real $|\mu_c| > 0.4$ eVto imaginary $|\mu_c| < 0.4$ eV. Note that in the vicinity of $|\mu_c| \geq 0.4$ eV a small change in the chemical potential yields a substantial change in the real value of the effective index of graphene as shown in the upper right part of Fig. 1. Graphene is electro-refractive in that region. On the other side, a small change in the chemical potential in both directions around $|\mu_c| = 0.4$ eV yields a substantial change in the imaginary value of the dielectric constant (i.e., the losses) and graphene is electro-absorptive in that region. Exploiting either the electro-refractive or the electro-absorptive behaviour of graphene lies at the heart of designing the microwave photonics phase-shifter. Tunability is achieved by suitable application of a voltage V_g to the graphene layer in combination with a dielectric substrate, since this changes the value of the chemical potential according to [11]

$$\left|\mu_c(V_g)\right| = \hbar \mathbf{v_F} \sqrt{\pi \left|\frac{CV_g}{e} - n_o\right|} = \hbar \mathbf{v_F} \sqrt{\pi \frac{C}{e} |V_g - V_o|} \tag{6}$$

where $V_o = 0.8$ V is the offset from zero caused by natural doping n_o due to the graphene-substrate interaction (we assume p doping), $C = \varepsilon_d/d$ is the effective capacitance per unit area, where d represents the substrate layer thickness, ε_d the dielectric constant of the combined graphene-substrate structure, and $\eta = C/e = 9 \times 10^{16}$ V^{-1}m^{-2} [6]. The relationship between the required chemical potentials and the carrier densities can be found by straightforward application of

$$n_s(\mu_c) = \frac{2}{\pi \hbar^2 v_F^2} \int_0^\infty x\left[f(x) - f(x + 2\mu_c)\right] dx. \tag{7}$$

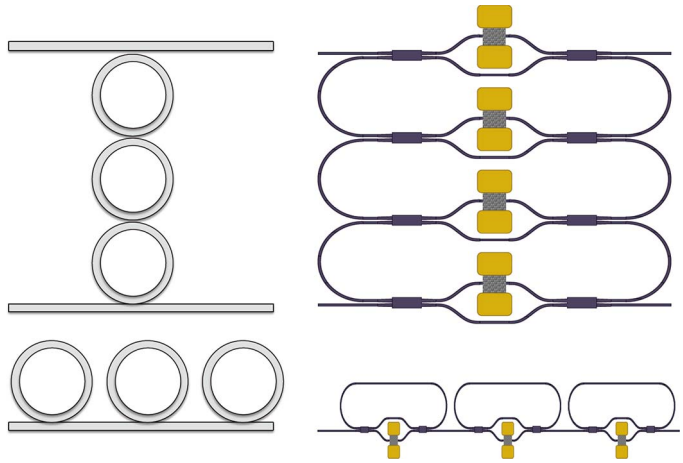

Fig. 2. Left: Diagrams of a CROW (upper) and SCISSOR (lower) cavity filter. Right: Proposed implementation of a reconfigurable CROW and SCISSOR using tunable 2 × 2 graphene MZI 3 dB couplers.

Graphene can be incorporated into silicon to implement graphene silicon waveguides (GSWs). One approach, shown in the lower left part of Fig. 1 consists in placing a monolayer graphene sheet on top of a silicon bus waveguide, separated from it by a thin Al_2O_3 layer. The presence of the graphene layer modifies the propagation characteristics (field profile, losses, and effective index) of the guided modes and these can be in turn, as mentioned above, controlled and reconfigured changing the chemical potential by means of applying a suitable voltage. In addition, all these properties are wavelength dependent; therefore, a complete description of how these parameters change in terms of chemical potential and wavelength is required. With the exception of very simple and unpractical waveguide configurations, this description requires the use of numerical and or mode solving techniques. For the waveguide shown in the lower left part of Fig. 1 a numerical procedure reported in [12], [13] yields the effective index and absorption losses versus the chemical potential for both transverse electric (TE) and Magnetic (TM) modes. The lower right part of Fig. 1 shows, as an example for $\lambda = 1550$ nm the effective index and the losses (in insets) versus the chemical potential for the TM fundamental mode.

3. Silicon Graphene Reconfigurable CROW and SCISSOR Structures

The right part of Fig. 2 shows the typical diagrams of a CROW [20] (upper part) and a SCISSOR (lower part) cavity filter respectively. Although the number of cavities in both structures can be arbitrary, in the figure we only show three. Note as well that the SCISSOR can have an upper waveguide bus, which we have not included in the figure. Throughout this paper we will assume that all cavities have the same length L, although in practice they can also be different. In the right part of the figure we show the design for the proposed silicon graphene versions of both designs respectively. A racetrack configuration has been selected where the coupling regions between the different cavities and those between the bus waveguides and the input cavities are implemented by means of a 3 dB tunable Mach–Zehnder Interferometer (MZI) as proposed by Madsen *et al.* [21]. This structure behaves as a tunable 2 × 2 coupler provided that the phase difference between the balanced arms (of total length L_{MZI}) of the MZI can be tuned by some external means. In practice it is customary to do so by exploiting the thermo-optic effect, but this results in an inherently slow tuning speed (several milliseconds). A fast phase shift and therefore coupler tunability can be achieved exploiting the electro-refractive region of the silicon graphene waveguide shown in Fig. 1, which corresponds to $|\mu_c| \geq 0.4$ eV. To do so, one of the two arms of the MZI structure is includes a portion of silicon graphene waveguide of length L_g.

The upper part of Fig. 3 shows a more detailed description of the tunable MZI device where all the relevant elements are displayed including the metal contacts to obtain the desired value of the chemical potential by the application of a suitable voltage according to (6).

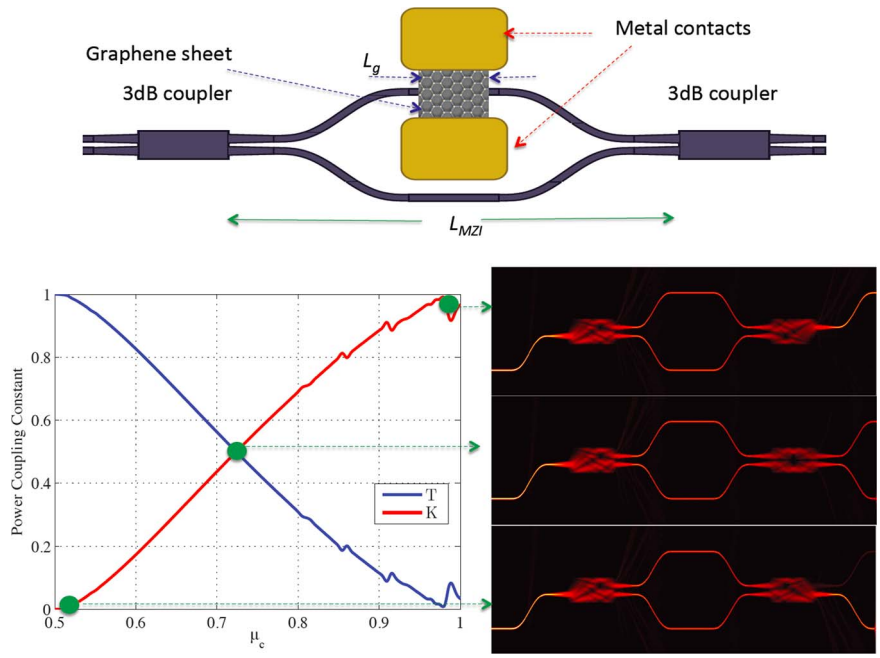

Fig. 3. Upper: Detailed diagram of the tunable MZI with all the relevant elements. Lower: Intensity transfer function of the MZI tunable 2 × 2 coupler as a function of the chemical potential when a $Lg = 100$ mm silicon graphene waveguide is included in one of its arms. Spatial field mode propagation is also depicted for selected points in the curve.

The lower left part of Fig. 3 shows the intensity transfer function of the silicon graphene MZI as a function of the chemical potential for the waveguide design of the lower left part of Fig. 1 and its corresponding effective index variation shown in the lower right part of Fig. 1. We have assumed for this case $L_g = 100$ μm. As it can be observed the whole range of possible values of equivalent coupling constant $(0 \leq K \leq 1)$ can be achieve by tuning the chemical potential from 0.5 to 1 eV, which correspond to carrier densities in the order of 20 to 60 $\times$ 10^{12} cm^{-2} [9]. This range can be decreased if the length of the silicon graphene waveguide is increased. For instance if $L_g = 200$ μm then $0 \leq K \leq 1$ is achieved by tuning the chemical potential from 0.5 to 0.72 eV. As it was found also in [11] for electro-refractive graphene modulators the transfer function of the MZI is not periodic with the chemical potential. The lower right part of Fig. 3 shows the spatial field propagation obtained by numerical computation of three relevant points in the transfer function curve K $= 0$ $(\mu_c = 0.5)$, K $= 0.5$, $(\mu_c = 0.7238)$, and K $= 1$ $(\mu_c = 0.967)$. The feasibility of tuning the coupling constant of the equivalent MZI 2 $\times$ 2 coupler allows the implementation of reconfigurable CROW and SCISSOR filters. Fig. 4 shows, for instance, the results obtained of a 5 cavity lossless CROW and SCISSOR structures. In all the cases, the racetrack cavities had equal length (650 μ_m).

Further control is possible if the tunability provided by the graphene variable MZI 2 $\times$ 2 couplers can be exploited to implement filter synthesis algorithms. For instance, an elegant continuous fraction technique has been derived in [22] that allows for the synthesis of CROW filters by means of the insertion loss method. We have employed the technique described in [22] to implement second, third and fourth maximally flat Butterworth filters using CROW structures. Fig. 5 shows the results obtained for the different filter orders taking the value of the chemical potential μc (equivalent coupling constant K) corresponding to the input coupler (from the input bus waveguide to the first cavity) as a parameter. The values of the rest of chemical potentials μ_{c1}, $\mu_{c2}, \ldots$(coupling constants K_1, $K_2, \ldots$) for the subsequent couplers can be related to this first one according energy coefficient relationships derived in [22, Tab. 1]. Table 1 gives the

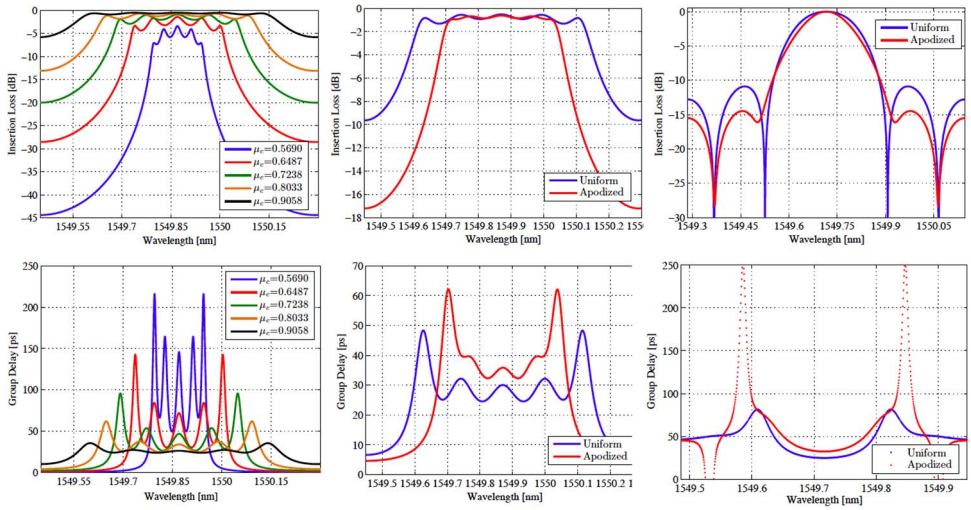

Fig. 4. Left: Transmission and group delay for a 5 racetrack uniform CROW including graphene tunable couplers for several values of chemical potential. Middle: Similar results for a 5 racetrack uniform (blue line) and apodized (red lines) CROWs. All the couplers in the uniform CROW have a $\mu_c = 0.85$ (K = 0.8) and the apodized CROW has the following values: $\mu_c = [0.8338\ 0.7432\ 0.7\ 0.7\ 0.7432\ 0.8338]$ (K = [0.7606 0.5501 0.4371 0.4371 0.5501 0.7606]). Right: Similar results for a 5 racetrack uniform (blue lines) and apodized (red lines) SCISSOR including graphene tunable couplers. All the couplers in the uniform SCISSOR have a $\mu_c = 0.569$ (K = 0.1). For the apodized SCISSOR, the following values are employed: $\mu_c = [0.5467\ 0.5544\ 0.5667\ 0.5667\ 0.5544]$ (K = [0.0546 0.0687 0.0950 0.0950 0.0687]). In all the cases, the racetracks have a cavity length of 650 microns and an FSR∼100 GHz, and only the detail of a single resonance is shown.

required values for each of the transfer functions displayed in Fig. 5. As it can be appreciated from Fig. 5 maximally flat response is obtained in all the cases with a better approximation to the Butterworth filter profile for higher Q (K < 0.3) and higher cavity count filters (which is actually the condition for which the partial fraction approximation of the CROW filter transfer function derived in [22] holds.

4. Discussion

The results obtained in Section 3 show that, in principle, the use of silicon graphene waveguides can be employed to implement tunable CROW and SCISSOR structures with fairly complex transfer functions. We now discuss on the orders of magnitude of the required voltages, the power consumption, and reconfiguration speed.

The required voltage ranges can be obtained from the chemical potential using (6). According to the results displayed in Fig. 3, covering a coupling constant range of $0 \leq K \leq 1$ with a tunable coupler with $L_g = 100$ mm requires a chemical potential range $0.5 \leq \mu_c \leq 1$ or, a voltage range of $2 \leq V \leq 8$ volt, that is, a voltage excursion of around 6 volt. In practice however and as shown in Section 3, high performance filters will not require values of chemical potential exceeding 0.73 eV. This further lowers the range of voltage to $2 \leq V \leq 4.3$ volt, that is, a voltage excursion of around 2.3 volts. Note that, according to (6) the voltage operation values will depend on the effective capacity, which, in turn can be altered by changing the oxide thickness in the waveguide structure. Regarding the power required by coupler this will depend on the value of the contact resistance between the electrode and the graphene sheet since the resistance of the graphene layer can be neglected [6]. Typical reported values are in the around $R = 600\ \Omega$ [6], which imply a power range in between 3.3 and 15.4 mW, that is a 12 mW margin to drive the coupler from $0 \leq K \leq 0.5$. Finally regarding the potential reconfiguration speed of the individual couplers this will be proportional to their *RC* time constant. Since typical values of the capacity are in the order of 0.2 pF [6] the expected reconfiguration speed is around 0.12 ns,

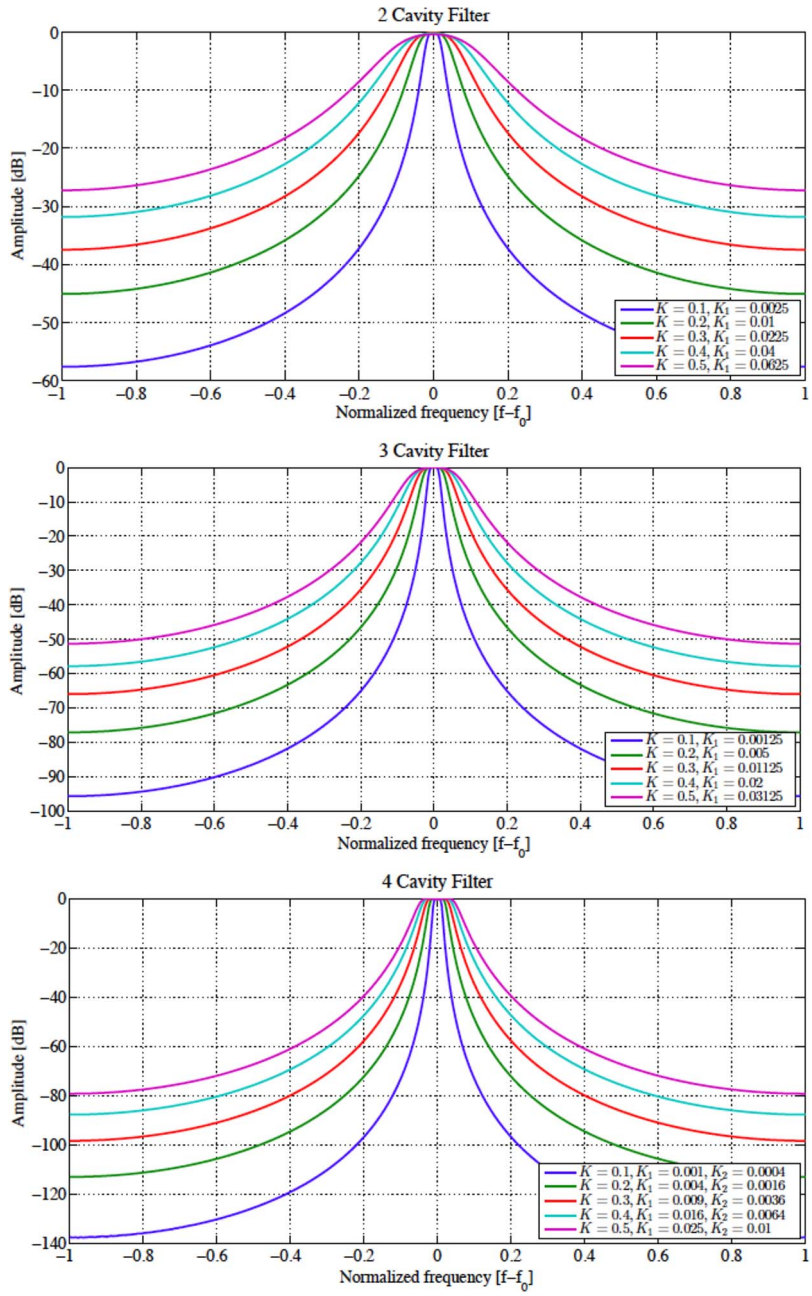

Fig. 5. Results for the synthesis of Butterworth filters using 2, 3, and 4 equal cavity length (650 μm) CROW structures and the partial fraction method of [20]. The required values for the chemical potentials in each case are given in Table 1.

which is at least three orders of magnitude faster than what is achievable with thermo-optic effects.

5. Summary and Conclusion

We have proposed, for the first time to our knowledge, the incorporation of graphene to integrated coupled resonator waveguides (CROWS) and SCISSOR devices to enable

TABLE 1

Required values for the chemical potentials in the 2 × 2 silicon graphene MZI variable 2 × 2 couplers for implementing of two, three, and four cavity butterworth filters

TWO CAVITY FILTER

K	K_1	μ_c (eV)	μ_{c1}(eV)
0.5	0.0625	0.7238	0.5516
0.4	0.04	0.6860	0.5388
0.3	0.0225	0.6487	0.5282
0.2	0.01	0.6106	0.5193
0.1	0.0025	0.5690	0.5120

THREE CAVITY FILTER

K	$K_1 = K_2$	μ_c (eV)	$\mu_{c1} = \mu_{c2}$ (eV)
0.5	0.0312	0.7238	0.5336
0.4	0.02	0.6860	0.5265
0.3	0.0112	0.6487	0.5200
0.2	0.005	0.6106	0.5159
0.1	0.0013	0.5690	0.5083

FOUR CAVITY FILTER

K	$K_1 = K_3$	K_2	μ_c (eV)	$\mu_{c1} = \mu_{c3}$ (eV)	μ_{c2} (eV)
0.5	0.025	0.01	0.7238	0.5298	0.5193
0.4	0.016	0.0064	0.6860	0.5235	0.5170
0.3	0.009	0.0036	0.6487	0.5187	0.5143
0.2	0.004	0.0016	0.6106	0.5148	0.5092
0.1	0.001	0.0004	0.5690	0.5072	0.5072

reconfigurable operation. The key element to achieve this is a tunable silicon graphene Mach–Zehnder interferometer (MZI) that acts as an equivalent variable 2 × 2 coupler, where the value of its coupling constant is changed by varying the chemical potential of a graphene section placed on top of one of its arms. Versatile operation including uniform, windowed, and maximally

flat reconfigurable transfer function has been demonstrated. Typical orders of magnitude related to required operating voltages, power consumption and reconfiguration speeds have been discussed.

References

[1] A. K. Geim and K. S. Novoselov, "The rise of graphene," *Nature Mater.*, vol. 6, no. 3, pp. 183–191, Mar. 2007.
[2] A. Vakil and N. Engheta, "Transformation optics using graphene," *Science*, vol. 332, no. 6035, pp. 1291–1294, 2011.
[3] B. Sensale-Rodriguez, R. Yan, L. Liu, D. Jena, and H. G. Xing, "Graphene for reconfigurable THz optoelectronics," *Proc. IEEE*, vol. 101, no. 7, pp. 1705–1716, Jul. 2013.
[4] F. Bonnacorso, Z. Sun, T. Hasan, and A.-C. Ferrari, "Graphene photonics and optoelectronics," *Nat. Photonics*, vol. 4, pp. 611–622, 2010.
[5] B. Sensale-Rodriguez, "Graphene based optoelectronics," *IEEE J. Lightw. Technol.*, 2014, to be published.
[6] M. Liu *et al.*, "A graphene-based broadband optical modulator," *Nature*, vol. 474, no. 7349, pp. 64–67, Jun. 2011.
[7] M. Liu, X. Yin, and X. Zhang, "Double-layer graphene optical modulator," *Nano Lett.* vol. 12, no. 3, pp. 1482–1485, Mar. 2012.
[8] Z. Lu and L. Zhao, "Nanoscale electro-optic modulators based on graphene-slot waveguides," *J. Opt. Soc. Amer. B, Opt. Phys.*, vol. 29, no. 6, pp. 1490–1496, Jun. 2012.
[9] M. Midrio *et al.*, "Graphene-assisted critically-coupled optical ring modulator," *Opt. Express*, vol. 20, no. 21, pp. 23 144–23 155, Oct. 2012.
[10] L. Yang *et al.*, " Proposal for a 2 × 2 optical switch based on graphene-silicon-waveguide microring," *IEEE Photonol. Technol. Lett.*, vol. 26, no. 3, pp. 235–238, Feb. 2014.
[11] C. Xu, Y. Jin, L. Yang, J. Yang, and X. Jiang, "Characteristics of electro-refractive modulating based on graphene-oxide-silicon waveguide," *Opt. Express*, vol. 20, no. 20, pp. 22 398–22 405, Sep. 2012.
[12] J. Capmany, D. Domenech, and P. Muñoz, "Silicon graphene waveguide tunable broadband microwave photonics phase shifter," *Opt. Express*, vol. 22, no. 7, pp. 8094–8100, Apr. 2014
[13] J. Capmany, D. Doménech, and P. Muñoz, "Graphene integrated microwave photonics," *J. Lightw. Technol.*, vol. 32, no. 20, pp. 3785–3796, Oct. 2014
[14] J. Capmany and D. Novak, "Microwave photonics combines two worlds," *Nature Photon.*, vol. 1, pp. 319–330, 2007.
[15] J. Yao, "Microwave photonics," *J. Lightw. Technol.*, vol. 27, no. 3, pp. 314–335, Feb. 2009.
[16] D. Marpaung *et al.*, "Integrated microwave photonics," *Laser Photon. Rev.*, vol. 7, no. 4, pp. 506–538, Jul. 2013.
[17] Y. Sano *et al.*, "Imaging molecular adsorption and desorption dynamics on graphene using terahertz emission spectroscopy," *Sci. Rep.*, vol. 4, 2014, Art. ID. 6046.
[18] N. Gruhler *et al.*, "High-quality Si3N4 circuits as a platform for graphene-based nanophotonic devices," *Opt. Express*, vol. 21, no. 15, pp. 31 678–31 689, Dec. 2013.
[19] G. W. Hanson, "Dyadic Green's function and guided surface waves for a surface conductivity model of graphene," *J. Appl. Phys.*, vol. 103, 2008, Art. ID. 064302.
[20] J. Capmany, P. Muñoz, J. D. Domenech, and M. A. Muriel, "Apodized coupled resonator waveguides," *Opt. Express*, vol. 15, no. 16, pp. 10 196–10 206, Aug. 2007
[21] C. K. Madsen and J. H. Zhao, *Optical Filter Design and Analysis*. New York, NY, USA: Wiley, 1999.
[22] B. E. Little, S. T. Chu, H. A. Haus, J. Foresi, and J-P. Laine, "Microring resonator channel dropping filters," *IEEE J. Lightw. Technol.*, vol. 15, no. 6, pp. 998–1005, Jun. 1997.